Merging computational fluid dynamics and machine

learning to reveal animal migration strategies

Simone Olivetti^{*}, Michael A. Gil[†], Vamsi K. Sridharan[‡], and Andrew M. Hein^{§ ¶}

4 Abstract

11

12

- 1. Understanding how migratory animals interact with dynamic physical environments remains a major challenge in migration biology. Interactions between migrants and wind and water currents are often poorly resolved in migration models due to both the lack of a high-resolution environmental data, and a lack of understanding of how migrants respond to fine scale structure in the physical environment.
- 2. Here we develop a generalizable, data-driven methodology to study the migration of animals through complex physical environments. Our approach combines validated Computational Fluid Dynamic (CFD) modeling with animal tracking data to decompose migratory movements into two components: movement caused by physical forcing, and movement due to active locomotion. We then use a flexible recurrent neural network model to relate local environmental con-

^{*}Southwest Fisheries Science Center, National Oceanic and Atmospheric Administration; Institute of Marine Sciences, University of California, Santa Cruz, CA 95060

[†]Department of Ecology and Evolutionary Biology, University of Colorado, Boulder, CO 80309; Southwest Fisheries Science Center, National Oceanic and Atmospheric Administration, Santa Cruz; Institute of Marine Sciences, University of California, Santa Cruz, CA 95060

 $^{^{\}ddagger}$ Southwest Fisheries Science Center, National Oceanic and Atmospheric Administration; Institute of Marine Sciences, University of California, Santa Cruz, CA 95060

[§]Southwest Fisheries Science Center, National Oceanic and Atmospheric Administration; Institute of Marine Sciences, University of California, Santa Cruz; Department of Ecology and Evolutionary Biology, University of California, Santa Cruz, CA 95060

[¶]for correspondence: simoneolivetti.eng@gmail.com, andrew.hein@noaa.gov

- ditions to locomotion behavior of the migrating animal, allowing us to predict a migrant's force production, velocity and trajectory over time.
 - 3. We apply this framework to a large data set containing measured trajectories of migrating Chinook salmon through a section of river in California's Sacramento-San Joaquin Delta. We show that the model is capable of describing fish migratory movements as a function of local flow variables, and that it is possible to accurately forecast migratory movements on which the model was not trained.
 - 4. After validating our model, we show how our framework can be used to understand how migrants respond to local flow conditions, how migratory behavior changes as overall conditions in the system change, and how the energetic cost of migratory movements depend on environmental conditions in space and time. Our framework is flexible and can readily be applied to other species and systems.
 - Computational Fluid Dynamics; Migration; Bionergetics; Machine Learning.

$_{\scriptscriptstyle 35}$ 1 Introduction

19

21

25

27

28

30

31

32

33

34

- Migration is an essential part of many animal life cycles (Dingle 2015). For
- animals that swim and fly, migration often involves not only long-distance nav-
- 38 igation and ecological interactions with conspecifics and predators, but also
- 39 complex interactions with the physical environment in the form of air and wa-
- ter currents (Smith, 2012, Dingle, 2015, Flack et al., 2018). The way migratory
- animals interact with abiotic currents can determine the energetic cost of migra-
- tion (Pennycuick, 2008) and even whether migration is feasible at all (Alexander,
- 1998, Pennycuick, 2003). Because climate change and anthropogenic habitat
- 44 alteration are modifying air and water currents at both small and large scales
- 45 (Boning et al., 2008, Kling and Ackerly, 2020, Silva et al., 2018), management

plans must increasingly consider how human activities influence the physical environment through which migrants travel (Thorstad et al., 2008). There is a growing recognition that managing migratory species must involve managing landscapes to facilitate successful migration (Silva et al., 2018, De Lucas, Janss, and Ferrer, 2004). However, to make informed decisions about how changes to the environment will alter the ability of animals to migrate, we need a deeper understanding of how air and water currents influence migratory physiology and also migratory behavior.

In the past, efforts to understand how migrants interact with abiotic forcing

have tended to take a migration physiology perspective, where the emphasis 55 has been on combining biomechanical models with physiological data to understand the cost of migration in flows (e.g., Martin et al., 2015). For example, 57 classic work on animal migration considered the energetic costs of large-scale mean wind or water currents on the cost of a migratory journey and on the fuel 59 loads required at stopovers, as well as the ranges migrants could achieve under favorable and unfavorable currents (Pennycuick, 2003, Pennycuick, 2008). More recently, several studies have analyzed physical data or models of wind or hydrodynamics in the context of animal migration (Weber et al., 2006, North et al., 2008, Arenas et al., 2015; Gao et al., 2015, Reddy et al., 2016). Nevertheless, a 64 major outstanding challenge in migration biology is understanding how migrant behavior and physical forcing by wind and water currents interact to determine how migrants move across a landscape, and the costs they incur when doing so. One of the limitations of many animal tracking data sets is that only the positions and movements (e.g., via animal-borne accelerometers) of the animal are recorded, and details of the physical environment through which the animal moves are unknown. Because of this, movements must often be studied and interpreted without knowledge of the physical forces and sensory cues that in-

fluenced the observed motion of the animal. This severely limits the types of questions about migration behavior that can be answered with movement data. While modern animal-borne sensors can aid in this problem (Hughey et al., 2018), at present, such sensors are often expensive and too heavy to be carried by small animals. Moreover, animal-borne sensors have the added limitation 77 that they record conditions only in the vicinity of the sensor, leaving the range 78 of conditions available to the animal elsewhere in the environment unknown. Here, we present an alternative approach to the problem of inferring the physical variables an animal experiences as it moves. This approach combines animal tracking data with high-resolution physical models of the region through 82 which the tracked animal moves. The essential data requirements are (1) animal tracking data describing the physical position of an animal or animals over time, (2) measurements of the structure of the physical environment (e.g., river bathymetry, local landscape topography), and (3) a collection of sample mea-86 surements of the physical variables one wishes to model (e.g., local water or wind velocity), preferably collected from the study region over the same range of conditions as those experienced by tracked animals. The latter two data sources are used to build a dynamic model of the physical environment that can then be used to infer the physical forces a tracked animal experienced at 91 each location in the tracking data set. The end result of fusing animal tracking data with the physical model is a data set containing positions, velocities, and 93 accelerations of each tracked animal (inferred from the tracking data), as well as estimates of the physical forces experienced by the animal at each point in time. Such data can then be used to infer how physical forces influence movement behavior, and to address a suite of questions related to the energetic output required to produced observed movements.

99 In what follows, we illustrate how to fuse animal tracking data and physi-

cal variables using, as an example, migratory juvenile Chinook salmon migrat-100 ing through a section of river in the Sacramento-San Joaquin Delta in Califor-101 nia. Tracking data consist of high spatial- and temporal-resolution tracks from 102 salmon as they move through a key segment of the migration route. To model 103 the flow environment these animals experience, we combine river bathymetry 104 data with flow measurements taken in several places throughout the study region 105 to develop a Computational Fluid Dynamics (CFD) model of water flow through 106 the entire study domain. We use the CFD model to estimate the dynamic fluid 107 environment experienced by each individual along its migratory trajectory. We show how this data set can then be used to estimate the force exerted on the 109 animal by moving water as well as the force produced by the animal through locomotion. Finally, to explore how cues from the physical environment – in 111 this case the flow cues experienced by fish – influence active swimming behavior, 112 we develop a recurrent neural network model to predict active locomotion as a 113 function of flow cues, and to forecast fish movement trajectories over the near 114 term. Taken together, the elements of our methodology allow one to explore a 115 broad suite of questions about how migrants interact with environmental flows 116 that have been challenging to address in past studies of animal migration. We 117 illustrate several applications of our approach by applying it to questions about 118 navigation behavior and migratory energetics over a wide dynamic range of flow 119 conditions. 120

2 Materials and Methods

The methodology we use to integrate tracking data with estimates of the flows animals experience is illustrated in Fig. 1. In addition to estimating physical variables at each point in time, the framework includes a step to predict movement behavior of animals as a function of these physical variables

(Fig. 1e,f) to determine the extent to which physical variables affect movement decisions. The data inputs to the modeling framework are animal trajectories 127 and the bathymetry and hydrodynamic data needed to build the CFD model 128 (Fig. 1a and 1b). The hydrodynamic data consist of two-dimensional (along-129 stream and lateral) near-surface river water velocity measurements collected 130 with four Acoustic Doppler Current Profilers (ADCPs) (see Section 2.1 below), 131 and river bathymetry obtained from the 2010 California Department of Water 132 Resources and the United States Geological Survey's 2m-resolution multibeam 133 sonar survey (Wang et al., 2018). Fish trajectories consisted of two-dimensional (along-stream and lateral) tracks obtained from the California Department of 135 Water Resources (see Section 2.1 below).

We use the hydrodynamic data as inputs to simulate the flow-field in the sec-137 tion of river system with sub-meter spatial resolution and one second temporal resolution using an Unsteady Reynolds-averaged Navier Stokes (URANS) CFD 139 model (Fig. 1a-c). We use the fish trajectories to first quantify the kinematics 140 of motion (i.e., the velocities and accelerations of the fish) and, subsequently, 141 the hydrodynamic information to quantify the dynamics of motion, i.e., the 142 drag forces experienced by the fish and the locomotion forces exerted by the 143 fish (Fig. 1d). We then model the locomotion force of each individual using the 144 information from the fish trajectories and local hydrodynamic forces by training 145 the neural network model describing fish locomotion behavior. Subsequently, 146 we employ the trained neural network for multivariate time-series prediction of locomotion forces as a function of the time series of hydrodynamic forces and 148 behavioral responses (Fig. 1e). After producing predictions of locomotory behavior, we used the drag force and the locomotion force predicted by the neural 150 network to predict each individual fish's trajectory (Fig. 1f).

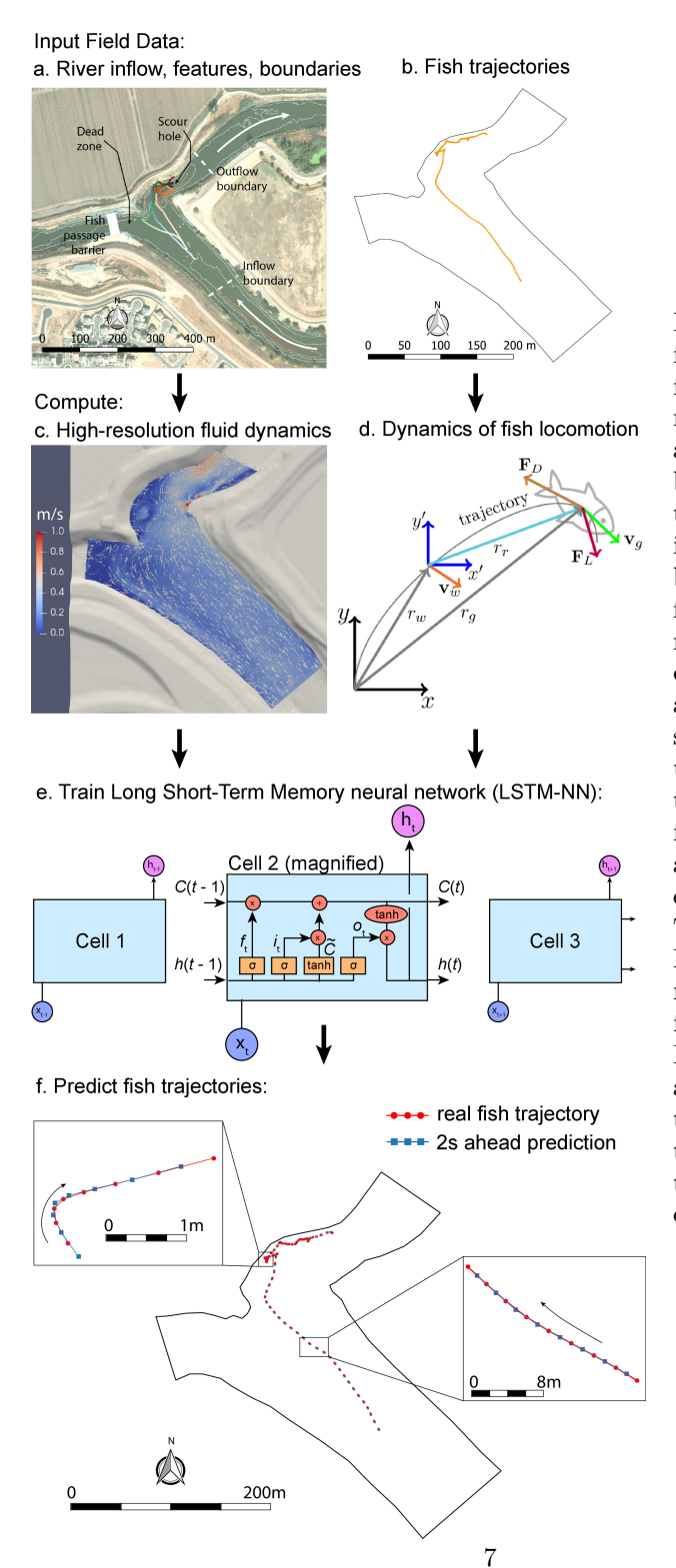


Figure 1: Modeling framework. a) Physical features of the environment and inflow data are collected along with b) migrant movement trajectories. c) Physical data are used to build Computational fluid dynamic (CFD) modeling of water flow. CFDpredictions are combined with observed fish movements used to decompose motion into drag-induced forcing by the flow and active locomotion. e) The Long Short-Term Memory Neural Network (LSTM-NN) model is developed to forecast locomotion. f) Locomotion predictions and flow are combined to forecast movement trajectories and predictions are compared to out-of-sample data.

2.1 Field data

Flow and animal tracking data were provided by the California Department 153 of Water Resources. These data were collected through a large collaborative study of a segment of the San Joaquin River within an agricultural and urban 155 watershed in the California Central Valley (study details provided in AECOM, 156 2015). The spatial locations of fish implanted with acoustic transmitters were 157 inferred using tag detections by a hydrophone array extending over roughly 158 1km of the San Joaquin River at the junction with Old River – a tributary – 159 and immediately downstream of the Southernmost extent of the Sacramento-160 San Joaquin Delta. The Delta is an inverted alluvial fan estuary formed at 161 the confluence of the Sacramento River from the North and the San Joaquin 162 River from the South, as well as numerous tributaries. This watershed is used by several species of salmonids of high conservation concern. Subpopulations of 164 Chinook salmon (Oncorhynchus tshawytscha) and steelhead (O. mykiss) traverse portions of the San Joaquin River and the Delta during their juvenile migration 166 to the Pacific Ocean (Williams, 2006), where they mature before returning as 167 adults (Sridharan et al., 2006 for a detailed description of the hydrometeorology 168 and hydrodynamics in the Delta). 169

Our study domain includes distinct regions as shown in Fig. 1a: (i) a 500m 170 long reasonably straight prismatic section of the mainstem San Joaquin River 171 about 150m downstream of a meandering section where the flow is Southeast 172 to Northwest, (ii) a junction at the Northwestern region of the straight section 173 where the Old River bifurcates to the West, and (iii) a sharp 90° bend Eastward 174 in the mainstem San Joaquin River. During the period when the study was 175 conducted, the bifurcation into Old River was blocked by a temporary earthen barrier (white box in Fig. 1a). The Eastward bend at the northern end of the 177 domain is characterized by an approximately 10m deep scour hole along the North bank where the flow separates and strongly recirculates before rejoining the freestream along the San Joaquin River (see Appendix D for the bathymetry of study domain).

Two-dimensional near-surface velocity fields were acquired by AECOM Tech-182 nical Services between 23 April and 30 May, 2012 using moored RDI Chan-183 nel Master side-looking broadband Acoustic Doppler Current Profilers (AD-184 CPs) operating at 600 Khz. Each cross-section was comprised of 2m-bins, 185 over which point velocity measurements were averaged over several minutes. A 186 5m-resolution flow field was reconstructed at fifteen-minute intervals through-187 out the study domain by first numerically computing the streamlines from the 188 Southermost ADCP cross-section and performing an inverse distance weighting interpolation using the velocity vectors obtained from the instrumented cross-190 sections (Stumpner, 2013a, Stumpner, 2013b). Fish trajectories were obtained from 424 Fall-run Chinook salmon implanted with injectable HTI hydroacoustic 192 tags (M800 and 795Lm models) which were detected at thirteen HTI hydroa-193 coustic detectors (model 590) deployed in an two-dimensional array throughout 194 the system. By colocating fish position using a minimum of four detectors, fish 195 positions were typically estimated at a precision of within 1m every two seconds 196 (AECOM, 2015). In the present study, we used 184 of these tracks that were 197 sufficiently long to be included in the neural network analysis. We applied our own post-processing pipeline to raw tag detections. This consisted of breaking 199 tracks from each fish into sub-segments if subsequent locations were separated by more than 30 seconds in time. Within each sub-segment, we smoothed tracks 201 using a third-order Savitzky-Golay filter with filter length of 22 seconds. Positions were also interpolated to a regular time interval of 2 seconds between 203 subsequent locations.

2.2 Fish behavior

206 2.2.1 Movement Kinematics

The first step in our workflow is describing the kinematics of fish movement. The 207 accuracy of position data in the depth dimension was poor, likely due to constraints on the positioning of hydrophones determined by the relatively shallow 209 average depth of the study region (AECOM, 2015). As a result, we were unable 210 to study movements of fish in the depth dimension, and we retained only the 211 horizontal coordinates of the position of each fish. Accordingly, tracks are rep-212 resented as 2-dimensional trajectories through the river section, and we consider 213 only horizontal components of the fish kinematics and dynamics. Henceforth, 214 we assign the East-West direction as the x-dimension and the North-South di-215 rection as the y-dimension. To keep track of the relative motion of fish and 216 flowing water, we define two reference frames: an inertial frame (x, y) fixed at 217 a point on the river bank and a relative frame (x', y') moving along the fish 218 trajectory with water velocity \mathbf{v}_w , see Fig. 1d. Given these reference frames, the position of a fish can be defined as follows: 220

$$\mathbf{r}_q = \mathbf{r}_r + \mathbf{r}_w. \tag{1}$$

Here, \mathbf{r}_g is the fish position with respect to the inertial frame (x, y), \mathbf{r}_r is the fish position with respect to the relative frame (x', y') and \mathbf{r}_w is the position of the relative frame with respect to the inertial frame. By recursively differentiating Eq. 1 with respect to time we obtain the velocity \mathbf{v}_g and acceleration \mathbf{a}_g of each fish as follows

$$\mathbf{v}_q = \mathbf{v}_r + \mathbf{v}_w,\tag{2}$$

$$\mathbf{a}_q = \mathbf{a}_r + \mathbf{a}_w. \tag{3}$$

 \mathbf{v}_g and \mathbf{a}_g are the fish's velocity (or overground velocity) and acceleration with respect to the inertial frame, \mathbf{v}_r and \mathbf{a}_r are the fish relative velocity and acceleration with respect to the relative frame and \mathbf{v}_w and \mathbf{a}_w are the velocity and acceleration of the relative frame with respect to the inertial frame. The latter quantities can also be interpreted as velocity and acceleration of a water parcel along the fish's trajectory. Eq. 2 and Eq. 3 are useful to decompose the fish motion (see Section 2.2.2 below).

233 2.2.2 Movement Dynamics

Once the kinematics are defined, we subsequently apply the momentum equation (i.e., Newton's second law of motion) to each fish to quantify its movement dynamics. In the horizontal plane, we identify two forces for each fish: locomotion force \mathbf{F}_L and drag force \mathbf{F}_D , see Fig 1d. We assumed that vertical forces such as gravitational force and buoyancy balance each other resulting in null vertical acceleration. Defining the fish's mass as m_{fish} , the fish dynamics can be summarized as

$$m_{fish}\mathbf{a}_q = \mathbf{F}_L + \mathbf{F}_D. \tag{4}$$

The drag force acts opposite to the relative motion of the fish moving with respect to the surrounding flow and it can be defined (Hoerner, 1965) as

$$\mathbf{F}_D = -\frac{1}{2}\rho_w A_f C_d ||\mathbf{v}_g - \mathbf{v}_w|| (\mathbf{v}_g - \mathbf{v}_w), \tag{5}$$

where ρ_w is the water density, A_f is the fish's wetted area and C_d is the drag coefficient, see Appendix A for how we calculate C_d and A_f . The term $\mathbf{v}_g - \mathbf{v}_w$ is the fish relative velocity \mathbf{v}_r with respect to the relative frame (see Eq. 2). The locomotion force can then be calculated by inverting the momentum equation, see Eq. 4. For this approach to be useful for understanding how instantaneous

fish behaviors contribute to their overall migration trajectories, we need infor-248 249 mation on the drag force at a spatial and temporal resolution commensurate with the tracking data. While m_{fish} can be obtained from the metadata as-250 sociated with the tracking experiments and \mathbf{a}_g can be directly obtained from 25 the tracking data, \mathbf{F}_D cannot be calculated at the desired resolution from the 252 fifteen-minute 5m-resolution interpolated ADCP \mathbf{v}_w fields. We therefore devel-253 oped the CFD model of the river system to estimate \mathbf{v}_w , and used this estimate to infer \mathbf{F}_D and compute \mathbf{F}_L . The details of the CFD modeling are described 255 in the following sections.

The tracking data consist of 184 fish tracks for a total of 129,830 location 257 points with a standardized temporal resolution of 2s. We show several example tracks in Fig 1b. Given the fish position $\mathbf{x}_g(t_n)$ from each track, the 259 fish velocity with respect to the inertial frame (see section 2.2.1) is $\mathbf{v}_g(t_n) \approx$ $(\mathbf{x}_g(t_{n+1}) - \mathbf{x}_g(t_n))/\Delta t$, where $t_n = [2, 4, 6, \dots]$ and $\Delta t = 2s$. The fish ve-261 locity with respect to the relative frame is obtained by reversing Eq. 2 such that $\mathbf{v}_r(t_n) = \mathbf{v}_g(t_n) - \mathbf{v}_w(t_n)$. $\mathbf{v}_w(t_n)$ is computed from the CFD results for each fish track (see section 2.3). Consequently $\mathbf{a}_r(t_n) \approx (\mathbf{v}_r(t_n) - \mathbf{v}_r(t_{n-1}))/\Delta t$. 264 With the kinematics defined thus, it is now possible to calculate the locomotion 265 force for each fish by combining Eq. 4 and Eq. 5 such that 266

$$\mathbf{F}_L(t_n) = \frac{1}{2} \rho_w A_f C_d ||\mathbf{v}_r(t_n)|| |\mathbf{v}_r(t_n) + m_{fish} \mathbf{a}_g(t_n) = f(\mathbf{v}_g(t_n), \mathbf{v}_w(t_n)).$$
(6)

It is important to notice that $\mathbf{F}_L(t_n)$ is a function of $\mathbf{v}_g(t_n)$ and $\mathbf{v}_w(t_n)$ as shown in Eq. 6.

2.3 Hydrodynamic variables

The next step in our workflow is to compute the drag force \mathbf{F}_D on the fish. Since \mathbf{F}_D is a function of \mathbf{v}_w (see Eq. 5) we simulated the flow dynamics of the river

using a three-dimensional CFD model based on Unsteady Reynolds-Averaged Navier-Stokes (URANS) equations. The river flow is considered incompressible and isothermal with the deflection of the water surface being represented by a 274 two-phase water-air Volume of Fluid (VOF) model. We used the openFOAM 275 solver interFoam (Deshpande, Anumolu, and Trujillo, 2012) to develop this 276 model. Although the tracking data we used are two-dimensional, we constructed 277 a three-dimensional CFD model to realistically represent the statistics of the 278 turbulence and the flow dynamics at the scour hole and in regions near the 279 channel banks. We assumed tracks were located within the uppermost cell of the CFD volume corresponding to approximately 0.3 meters below the water 281 surface.

283 2.3.1 Solver and Model Parameters

The interFoam solver in openFoam implements the continuity and momentum 284 equations for isothermal and incompressible flows along with an additional equation tracking the fraction of air within each parcel of water. The URANS models 286 requires turbulence closure equations in order to be a well-posed PDE system 287 (Menter, 1994). We used the $k-\omega$ equations to represent the statistics of the 288 unresolved turbulence. The boundary conditions for the velocity and the water 289 elevation are based on field measurements, see Section 2.1. The empirical flow velocity time-series is available at the inlet section for the three-month period 291 from March to May with a time resolution of 15 minutes supersampled linearly at 2s intervals. 293

2.3.2 Modeling active locomotion: a neural network approach

The final step in our workflow (Fig. 1e,f) is to develop a model describing how fish locomotion depends on features of the environment, including the hydrodynamic forces the animal experiences as it moves through the water. The details

of sensory integration, processing, and decision-making during navigation are poorly understood for most migratory species, including migratory fishes. To avoid making *ad hoc* assumptions that might arbitrarily restrict the form of the relationship between physical variables and movement behavior, we modeled effects of flow on movement behavior using a flexible approach for time-series prediction, the Long Short-Term Memory Neural Network (LSTM-NN).

We selected the LSTM-NN as a reasonable model of movement behavior for 304 two reasons: first, in the past, LSTMs have been used successfully to model 305 movements of vehicles and pedestrians (e.g., Xue, Huynh, and Reynolds, 2018, Altché and De La Fortelle, 2017). Second, there is detailed documentation 307 in the literature (Kang and Choi, 2005) on how LSTMs are implemented in TensorFlow (Abadi et al., 2015). This existing software implementation makes 309 LSTMs a convenient modeling tool for describing the relationship between physical variables and migrant behavior when no a priori model exists. Details of 311 the underlying structure of the LSTM and how it maps inputs to outputs is 312 given in the Appendix D. In the Discussion, we further elaborate on the pros 313 and cons of LSTM and the situations in which it is likely to provide a good 314 model of navigation behavior. 315

In the current application, we use the LSTM to predict the locomotory force produced by migrating fish at each time step. We take, as input to the network, the fish's overground velocity, \mathbf{v}_g , and the water velocity, \mathbf{v}_w , because $\mathbf{F}_L = f(\mathbf{v}_g, \mathbf{v}_w)$ as shown in Eq. 6. This assumes the fish could measure overground velocity, which could be accomplished, for example, through visual means, by estimating the optic flow of visual features on the benthos (e.g., the river bed itself, submerged debris or aquatic vegetation). In the past, environmental variables such as water acceleration, hydrostatic pressure (Goodwin et al., 2014), turbulent structures (Lacey et al., 2012), turbulent kinetic energy

intensity (Gao et al., 2015), and circulation around the fish (Oteiza et al., 2017) have been used to explain fish movement behaviors. We decided to use the 326 water velocity experienced by the fish because the river system under consider-327 ation is characterized by a relatively low turbulent kinetic energy content, and 328 because other mechanisms of behavior response to variables such as the local 329 shear or circulation are not understood in complex environmental flows. More-330 over, exploratory analyses including other variables in LSTM-NN training did 331 not indicate improved performance. 332 The resulting trained LSTM-NN is a function that relates the overground 333 velocity and water velocity experienced by a migrating fish at some time t_{n-1} 334

$$\mathbf{F}_L(t_n) = LSTM(\mathbf{v}_q(t_{n-1}), \mathbf{v}_w(t_{n-1})), \tag{7}$$

where t_n is the discrete time-step with n = [0, 1, ..., N - 1, N]. We note that the use of \mathbf{v}_g in this formulation allows us to explicitly model the locomotion of the fish as a function of its memory of its response to the local environment, as well as its current sensory experience. Details of LSTM-NN structure and how inputs map to predictions are given in Appendix C.

to the locomotion force produced by that fish at time t_n :

$^{_{341}}$ 2.4 LSTM-NN fitting, predictions, and out-of-sample test- $^{_{342}}$ ing

We used the LSTM-NN module available in TensorFlow (Abadi et al., 2015) for predicting \mathbf{F}_L . The training data set consisted of the time-series of overground velocities of fish and water velocities along the fish tracks. Furthermore, we used the time-series related to the observed components of the locomotion force $F_{L_x}(t_n)$ and $F_{L_y}(t_n)$ computed with the field data, see Eq. 6, as reference output for the LSTM-NN training. We optimized the LSTM-NN settings to

minimize the average error of ΔF_{L_x} and ΔF_{L_y} , where Δ is the difference between the predicted and actual value. We tested a number of LSTMs-NNs with 350 an increasing number of cells and used the k-Nearest-Neighbor method (Arya 351 et al., 1998) to select the architecture with the optimal number of cells (see 352 Appendix C). We found an LSTM-NN with 112 cells to be the optimal con-353 figuration, because it produced ΔF_{L_x} and ΔF_{L_y} with minimal average error. 354 After the end of the cascade of LSTM-NN cells, we included a dense layer of two 355 rectified linear activation functions, ReLU, to output the model results (Abadi 356 et al., 2015). The length of the training data set was 60% of the original data 357 set subdivided in 72 batches; the total length of the data set consist of 129,830 358 data points. We trained the LSTM over 30 epochs.

560 2.5 Forecasting fish movements

Once the LSTM-NN model of $\mathbf{F}_L(t_n)$ is fitted to training data, it can be used to predict migrant trajectories by applying the forward Euler method to Eq. 4 as follows:

$$m_{fish} \frac{\mathbf{v}_g(t_n) - \mathbf{v}_g(t_{n-1})}{\Delta t} \approx m_{fish} \mathbf{a}_g(t_n) = \mathbf{F}_L(t_n) + \mathbf{F}_D(t_n),$$
 (8)

Hence, considering Eq. 2 and Eq. 5

$$\begin{cases}
\mathbf{F}_{L}(t_{n}) = LSTM(\mathbf{v}_{g}(t_{n-1}), \mathbf{v}_{w}(t_{n-1})) \\
\mathbf{v}_{g}(t_{n}) = \mathbf{v}_{g}(t_{n-1}) + (\mathbf{F}_{L}(t_{n}) + \mathbf{F}_{D}(t_{n})) \frac{\Delta t}{m_{fish}} \\
\mathbf{x}_{g}(t_{n}) = \mathbf{x}_{g}(t_{n-1}) + \mathbf{v}_{g}(t_{n}) \Delta t
\end{cases} \tag{9}$$

The initial conditions $\mathbf{v}_g(t_0)$, $\mathbf{v}_w(t_0)$ and $\mathbf{x}_g(t_0)$ are determined from the corresponding field data. This scheme can be used both to predict fish velocities and trajectories in-sample, and to predict entirely new trajectories, given the

369 3 Results

3.1 CFD results

We used the CFD model of the study domain to compute flows over the duration 371 that fish were present. In Fig. 2a, we show a snapshot of the water velocity 372 field in the horizontal section near the water surface (where the fish trajectories are assumed to be contained). The contour colors represents the water velocity 374 magnitude, while the vectors represent the direction of local flow. The southeast 375 region close to the inlet is characterized by a flow that tends to be uniform. In 376 contrast, the northwest region close to the barrier shows a large area of flow 377 recirculation; two counter-rotating vortexes appear along the barrier Fig. 2b. A 378 vortex rotating in the counterclockwise direction on the northern bank is visible 379 in Fig. 2c. The formation of this vortex is due to the sharp bend of the river course and associated scour hole, causing the flow to recirculate along the north 381 bank. We validated the CFD model by comparing the velocity profiles from the numerical simulation against the velocity profiles from the field measurement; 383 we show in Fig. 2d and 2e that the CFD results (lines) are in good agreement 384 with the ADCP measurements from two cross sections which include a typical variation of $\pm 5.8 cm/s$ within each velocity bin (dots; AECOM, 2015).

3.2 Fish migration behavior and LSTM model predictions

The tracking data provided is an extensive collection of fish velocity and trajectory estimates from across the study domain. By applying the velocity decomposition introduced above to the fish trajectory data and CFD-generated flow velocity predictions, we were able to estimate the distinct contributions of

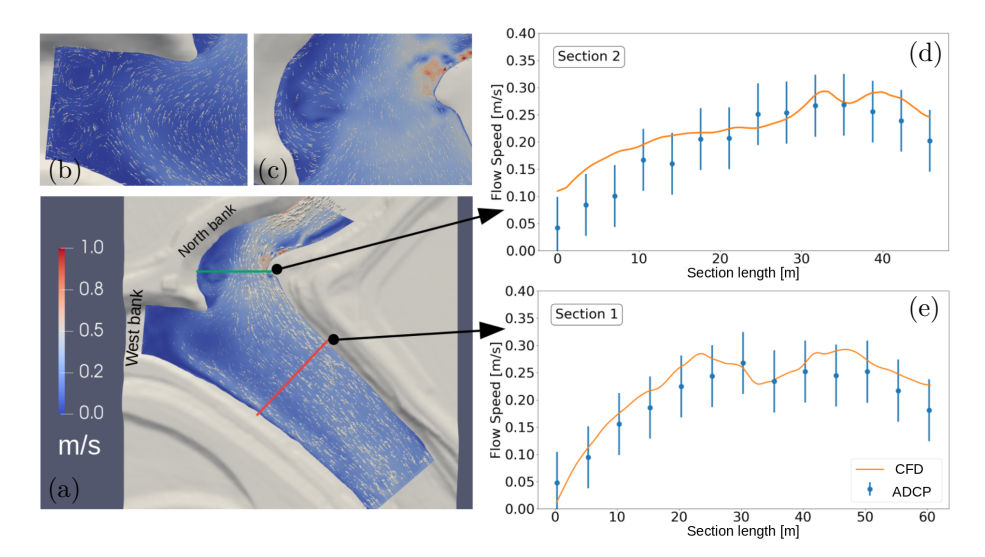


Figure 2: a) Snapshots of the velocity field magnitude at one point in time. The color bar indicates flow magnitude in units of m/s. Lines through the domain show cross-sections used for model validation. Red line: Section 1 (shown in panel e). Green line: Section 2 (shown in panel d). b) Zoomed in view of the Western bank showing regions of weak recirculation flow. c) Zoomed in view of the Northern bank showing a vortex. d) Comparison between CFD flow predictions (line) and water velocity magnitude measured by ADCP (blue dots and error bars) in Section 2. Profiles averaged over 30 minutes. e) Comparison between CFD predictions and data.

water flow and migrant locomotion to the observed overground velocity of each 392 migrating animal. In Fig. 3b, we show the probability density function (pdfs)393 of the magnitudes of the fish overground velocity, $||\mathbf{v_g}||$, and the fish relative velocity $||\mathbf{v_r}||$ (i.e., the animal's velocity relative the the moving water), as well as 395 the magnitude of water velocity at observed fish locations $||\mathbf{v}_{\mathbf{w}}||$. Note that the 396 overall magnitude of relative velocity of the fish – the component of velocity due 397 to active locomotion – often exceeds the magnitude of water velocity, indicating 398 that fish regularly swim at speeds that are higher than the speeds of the flows in 399 which they are swimming. This can be seen more directly in the distribution of 400 the ratio of relative velocity magnitude to the overground velocity magnitude, 401 Fig. 3a. The right tail of this distribution shows cases where fish are swimming 402

at speeds that far exceed the speed of local water movement.

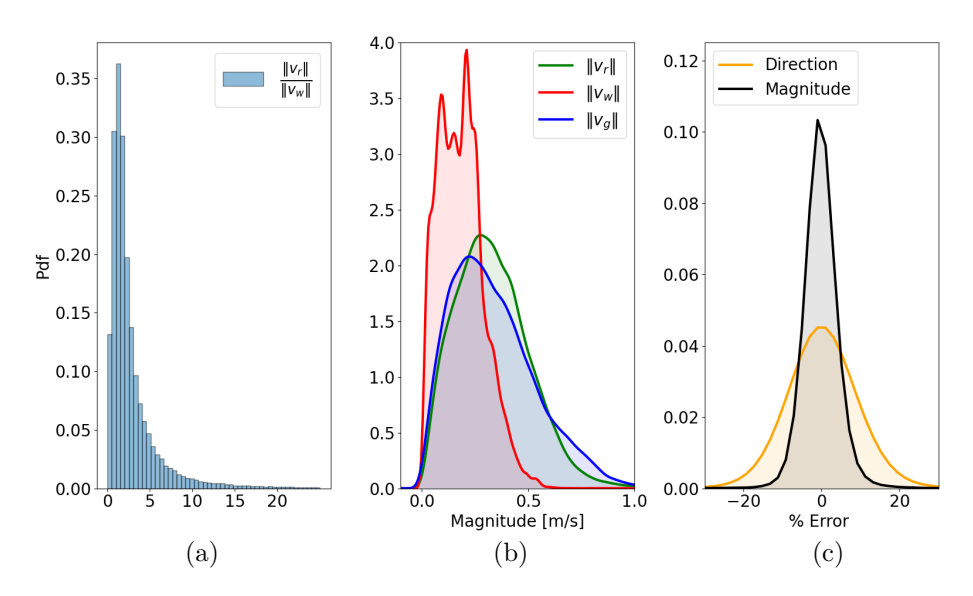


Figure 3: Empirical velocity data and LSTM-NN prediction performance. a) Pdf of the ratio of the magnitudes of the fish relative velocity to the water velocity. b) Pdfs of magnitude of the fish relative and overground velocity (green and blue distributions, respectively) and pdf of water speed at fish locations computed from CFD model (red distribution). c) Pdfs of prediction errors from the LSTM model shown as percentage error in predicted direction (orange distribution) and magnitude (grey distribution) of locomotion force.

Employing Eq. 6, velocity estimates can be used to estimate the locomotory 404 force produced by each fish to achieve its observed motion. The LSTM-NN 405 model of locomotion accurately predicted this locomotory force in the 51,932 406 data points (40% of the original data set) that were held out during training, 407 Fig. 3c. Typical errors for direction are within 20% of observed values, and 408 magnitude estimates are typically accurate to well within 10% of observed val-409 ues, Fig. 3c. Our results indicate that our model of fish swimming behavior is able to predict this behavior for times and locations on which the model was 411 not trained (i.e., on the out-of-sample data). 412 Given a prediction for the locomotory force, the equation system in Eq. 9 413

Given a prediction for the locomotory force, the equation system in Eq. 9 can be used to predict a fish's trajectory, $\mathbf{x}_g(t_n)$, in addition to the locomotion

415 forces, accelerations, and velocities.

We show the distributions of error in predicting position prediction measured in body length for several time ahead predictions, e.g. from 2s up to 30s (predictions shown are for 51,932 data points held out-of-sample during training)

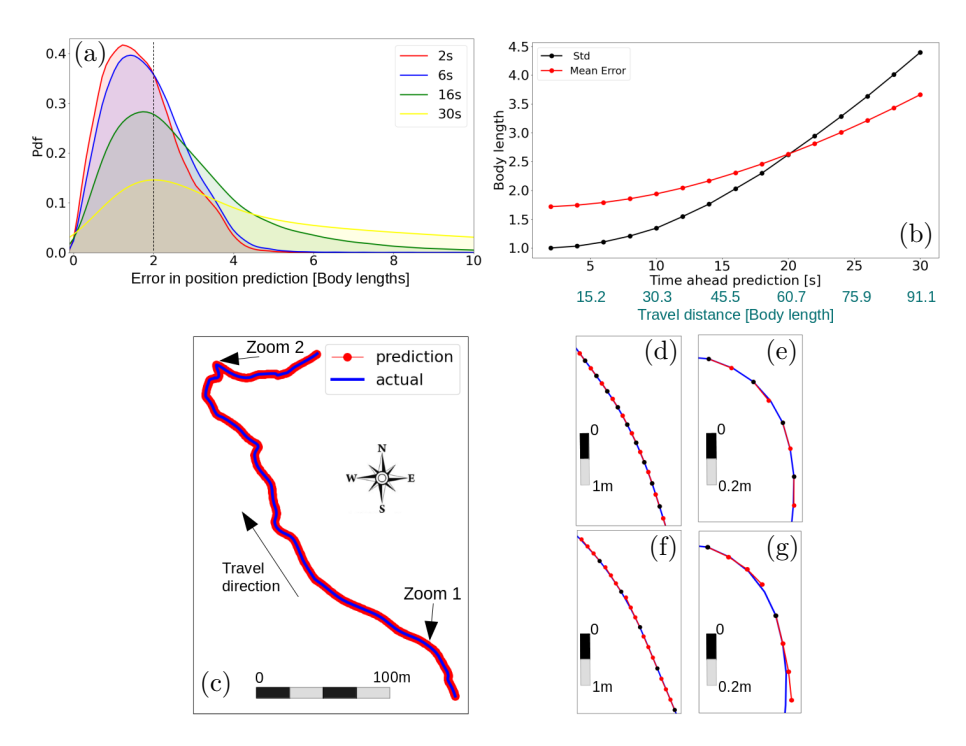


Figure 4: Trajectory prediction performance over different forecast time horizons. a) Pdfs of the error in predicting the position of the fish [in body lengths] for several of the prediction horizons. The vertical line at two body lengths indicates that the mode of the error in predicting fish positions is well contained for even large forecast time horizons. b) Mean error (red) and standard deviation (black) in predicting the position over forecast horizon (time in seconds) and average distance traveled by the fish (scale in green [in body lengths]). c) Example of a single trajectory prediction. Blue line shows observed trajectory; red points show predicted trajectory for 2s-ahead predictions. d) Zoomed into a straight section of the track (zoom 1) for 2s-ahead prediction. Black points show an initial location of the fish from which the Eq. 9 is initialized. Red points show predicted location 2s-later e) Zoomed into a curved section of the track (zoom 2) for 2s-ahead prediction. f) and g) 6s-ahead predictions zoomed into the sections shown in d) and e) respectively. Colors and symbols in e), f) and g) are as in d).

in Fig. 4a; while the tail of the error distribution includes significantly larger 419 errors as the prediction horizon increases, the mode of the error distribution 420 only grows by roughly one body length when moving from a prediction horizon 421 of 2 seconds to a horizon of 30 seconds. Red and blue distributions in Fig. 4a 422 show 2s-ahead and 6s-ahead predictions, illustrating that increasing the fore-423 cast horizon from 2 to 6 seconds does not result in a dramatic decrease in the 424 quality of predictions. Nevertheless, the discrepancies between the observed and 425 predicted trajectories do continue to grow as the prediction horizon is increased 426 as one would expect. In Fig. 4b, we show the dependence of the mean and stan-427 dard deviation of the error in predicting position on the forecast horizon. Up to 428 forecast horizons of 30 seconds, the mean prediction error remains below four fish body lengths. It is worth noting that the mean and standard deviation of 430 prediction error represent a small fraction of the typical travel distance during any given forecast horizon. For example, in 30s the average travel distance is 432 91.1 body lengths while the mean error is about 3.5 body lengths, green scale 433 in Fig. 4b. In Fig. 4c, we show a sequence of predictions along the length of 434 a long trajectory. In Fig. 4c the blue line is the actual trajectory of a tagged 435 fish while the red dots are the 2s-ahead predictions; this fish trajectory consists 436 of 455 points corresponding to 906s of the fish's trajectory through our study 437 region. We zoom into two parts of the trajectory which are structurally different from each other: a relatively straight section in Fig. 4d and a sharply curving 439 section in Fig. 4e. In these plots, the black dots are initial locations to initialize the model in Eq. 9. In both sections of the track, there is close alignment 441 between the observed and predicted trajectory points. In Figs. 4f - 4g, we show the same sections of the track for 6s ahead predictions (3 time-steps ahead); 443 while the accuracy tends to decrease as the prediction horizon increases, errors remain reasonably bounded, even in the highly curved region of the trajectory. 445

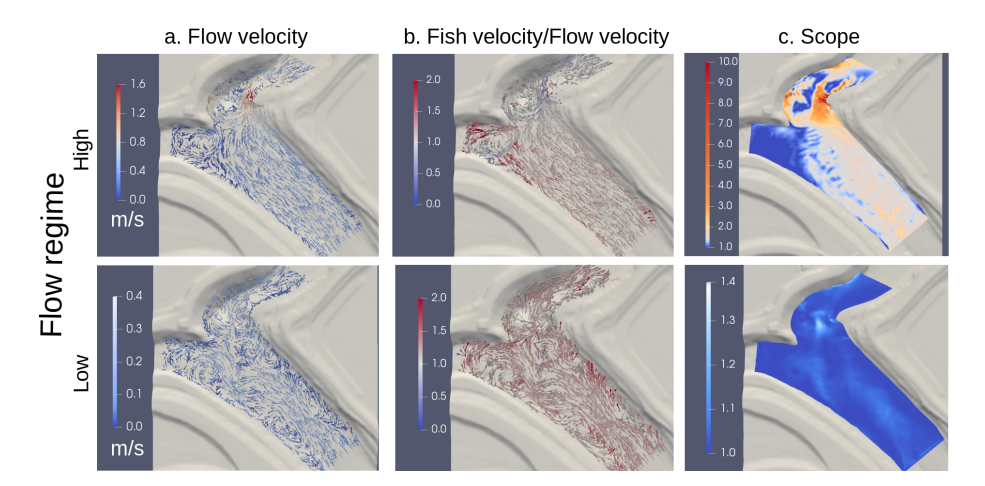


Figure 5: Predicted water flow, velocity ratio and locomotory scope under high (upper panels) and low (lower panels) net flow conditions. a) Flow velocity field. b) Ratio of the relative velocity of the fish to the water velocity. c) Locomotory scope, S_L . Note large differences in range of predicted scope between high (upper) and low (lower) flow conditions.

By combining the CFD model to predict flow, and the LSTM-NN to predict 446 fish locomotion in response to flows, one can explore a wide range of questions 447 about how flow and locomotory behavior of animals interact under different 448 conditions. For example, by exploiting the first two equations in Eq. 9, it is 449 possible to estimate the movements of fish across the entire flow domain for 450 different environmental conditions of interest. In Fig. 5a, we show snapshots of 451 the water velocity vector field in the river system during the period of lowest and 452 highest outgoing flows, respectively. In Fig. 5b, we show the "relative swimming 453 velocity", R_{fw} , defined as the ratio of the magnitudes of relative velocity of fish 454 and the water velocity, for the same flow conditions shown in Fig. 5a. Two 455 key patterns are immediately evident. First, the relative swimming velocities of the fish regularly exceed water velocity throughout much of the domain. This 457 predicted spatial pattern is consistent with the empirical observation shown in Fig. 3a-b that the observed relative swimming velocities regularly exceed 459

water velocity. Moreover, this demonstrates the degree to which fish movements 460 appear to be driven by active swimming behavior rather than simple passive 461 forcing by the flows. The second pattern evident in Fig. 5b is that there is 462 strong spatial heterogeneity in the ratio of fish to water velocities, and these 463 spatial patterns change as the overall flow transitions from weak to strong. For 464 example, during low flows, the relative swimming velocity is greatest in the open 465 channel, upstream of the bend. During high flows, relative swimming velocity 466 is much slower in this same region. During high flow, the relative velocities of 467 fish are smaller than the water velocity in the regions of high circulation near the channel bifurcation, whereas this pattern is not evident at low flows. 469

To determine the impact this spatial and flow-dependent variation in behavior has on migration energetics, we can estimate the rate of power output 471 required to achieve predicted movements across the domain. We do this by defining a quantity we will call "locomotory scope," $S_L = 1 + \mathbf{F}_L \cdot \mathbf{v}_r / RMR$, 473 which characterizes the power output required to fuel resting metabolism and 474 locomotion, normalized by the resting metabolic rate (RMR) (see Appendix A 475 for RMR calculation). The locomotory scope is a measure of the power output 476 of an animal measured in units of resting metabolic rate. Thus, a locomotory 477 scope of one corresponds to a case where an individual devotes no power to 478 locomotion, whereas a value of five corresponds to a case where the total rate 479 of power output (including resting metabolism) is five times resting metabolic 480 rate. Note that locomotory scope as it is defined here is not the same as aerobic 481 scope because we neglect any power loss due to inefficiencies in force produc-482 tion, and we do not consider other sources of power consumption (e.g., specific dynamic action) that could be relevant during migration. Thus, locomotory 484 scope should be taken as a lower bound on the relative power output required 485 during movements. 486

Our analysis of predicted locomotory scope reveals strong spatial patterns in 487 power output as well as strong differences in patterns across specific instances of low and high flow conditions, Fig. 5c. Under low flow conditions, locomotory 489 scope was generally below 1.5, indicating that the power required to produce 490 predicted migratory movements across the domain was generally less than half of 491 the resting metabolic rate of migrants. The highest relative power outputs were 492 predicted to be along the center of the main channel, upstream of the channel 493 bend, and in a region of relatively high circulation near the eastward channel 494 bend, Fig. 5c. In strong contrast to these patterns, locomotory scope during high flows was as large as 10 in some regions of the domain, indicating that 496 predicted movements in those regions required total power outputs 10 times higher than resting metabolic rate. The highest rates of power output were 498 predicted to be in the region of strong flow recirculation near the eastward channel bend and along the eastern bank in the same region. However, even 500 outside of these regions the locomotory scope exceeded a value of 1.5 throughout 501 much of the domain. One might expect migrants to take advantage of strong 502 oceanward flows in the high flow conditions by drifting passively rather than 503 swimming actively. To the contrary, our model suggests that migrants generally 504 use far more power under high flow scenarios, particularly in local regions of 505 strong unsteady flow. This is due, at least in part, to the fact that in weak flows, the locomotion force tends to be biased in alignment with the direction of 507 local water flow (Appendix A), whereas in more powerful flows, fish locomotion is aligned opposite or orthogonal to the direction of local water flow. 509

510 4 Discussion

Here, we have developed a general methodology to combine quantitative estimates of a turbulent environment with measurements of the movements of

animals to better understand migratory behavior in the wild. Our methodol-513 ogy combines animal tracking data with high resolution physical modeling of 514 environmental flows – here achieved using computational fluid dynamics – to 515 estimate the dynamic flow environment migrants experience and determine the 516 component of force of migratory movements due to active locomotion by the 517 animal. Finally, we employ recurrent neural network methods to relate the 518 physical conditions experienced by the migrant to locomotion behavior, and 519 use this model to forecast movements over times and conditions outside those 520 included in the training data. 52

Reconstruction of the local physical environment and decomposition of active 522 and passive components of movement have the potential to offer new insights into the processes that influence the movements of migrating animals in complex 524 environments. This approach extends recent work to characterize how migrants move in relation to coarser-scale environmental flows such as water currents and 526 regional wind patterns (e.g. the use of favorable prevailing winds and fast air 527 streams by migrating insects, Alerstam et al., 2011). Our approach also holds 528 significant promise as a tool for management of migratory species because, af-529 ter careful testing on out-of-sample data, our framework allows one to make 530 predictions about both the physical and behavioral consequences of modifying 531 the migratory environment, for example by raising or lowering flow, altering the 532 bathymetry or course of the river, or installing equipment such as water diver-533 sion facilities along the migration route (Thorstad et al., 2008, Silva et al., 2018). Although we have applied our framework to migratory fish in a river system, 535 the same methods could be used to understand migratory strategies of flying species by combining high-fidelity tracking during flight (Ling et al., 2018) with 537 CFD modeling of environmental features of interest (e.g. wind turbines, Martin et al., 2017) or physical modeling of turbulent convective flow in the atmospheric 539

boundary layer (Reddy et al., 2016). It is well known that flying animals also respond to local air flows (Scacco et al., 2019, Shepard, Ross, and Portugal, 2016 and Dabiri, 1993); however, constructing and validating models of air flow 542 poses some unique challenges. For example, it is often challenging to collect high-resolution time-varying data on air currents in the atmosphere that can be 544 used during model validation. For small-scale flow phenomena such as boundary layer flows over localized topography and built-up areas on the order of a few hundred square-meters to a few square kilometers, wind-tunnel experiments over 547 downscaled models can provide validation data sets for high-resolution URANS and LES models of atmospheric flow (e.g., Kellnerová et al., 2018 and Jimenez 549 and Moser, 1998). For flows distributed over larger open areas, on the order of tens of square kilometers, a combination of wind-vane, flux tower and LiDAR 551 and Radar measurements may be used to produce reliable estimates of the air currents (Friedrich et al., 2012 and Madala et al., 2015). An alternate strategy 553 more recently has been to dynamically or statistically downscale global circula-554 tion models to spatial-temporal resolutions required for regional-scale analysis 555 and validate these downscaled models using a regional network of weather sta-556 tions (Winstral, Jonas, and Helbig, 2017 and Wagenbrenner et al., 2016). For 557 many physical modeling methods, open source software packages are readily 558 available (e.g., openFoam), as are packages for constructing statistical models 559 (e.g., R, TensorFlow) of migration behavior once the locomotion component of 560 migratory movements has been computed (Fig. 1e,f).

Computational fluid dynamics, and computational modeling of the flow environment more generally, have already proven to be useful for studying environmental flows in the context of animal migrations. For example, Gisen, Weichert, and Nestler (2016) developed a 3D CFD model of a hydropower dam tailrace using a Detached-Eddy Simulation turbulence model to evaluate impacts on

migrants. Reddy et al. (2016) developed a computational model of thermals in the atmospheric boundary layer to study how soaring birds navigate complex turbulent motion of air. Gualtieri et al. (2019) modeled fish migration through 569 a river system as particles characterized by two bioenergetic parameters, one re-570 lated to the drag force a fish experienced and one related to the energy needed 571 by a fish to remain in a specific location. Similar assumptions were adopted 572 by Ramón, Acosta, and Rueda (2018) who studied the hydrodynamic drivers 573 of juvenile salmon movements using CFD to compute the flow field across a 574 river system. Although Gualtieri et al. (2019) and Ramón, Acosta, and Rueda (2018) modeled fish as passive particles dragged by the river flow, as we show 576 here, even small migratory fish can swim very actively, and in many cases, their locomotion force production is significant. Indeed, our analysis of relative ve-578 locity of fish and water (Fig. 5) shows that the component of ground speed due to active locomotion is often greater in magnitude than the water speed, even in 580 relatively fast flows. Our findings corroborate results from other systems (e.g., 581 Arenas et al., 2015), and suggests more generally that even small migratory an-582 imals such as the juvenile salmon considered here (mean length 112 mm) spend 583 significant amounts of energy on locomotion, even when the net direction of 584 environmental flow aligns with the direction of migration. 585

Several researchers have begun using CFD models to attempt to understand how migrants navigate complex physical environments at spatial and temporal 587 resolutions similar to those considered in our study. For instance, Goodwin et al. (2014) used a steady-state RANS CFD model to compute water field 589 velocity in combination with an ad hoc fish behavioral model to represent fish movements in the vicinity of hydropower facilities. Gao et al. (2015) used a similar approach for a slot fishway, applying a parametric model of fish movement. Martin et al. (2017) combined a CFD model of a wind turbine and aerody-593

586

591

namic modeling of bat flight to understand how flying bats might interact with the forces produced by wind turbines. In the present study, we extended the ap-595 proaches of these past models by developing a URANS CFD model to compute 596 time-dependent flow variables. We employed a time-dependent CFD model be-597 cause the flow-field through complex channel morphologies like the one studied 598 here can be extremely dynamic, particularly in river and estuary systems where 599 flows can change due to a variety of reasons including precipitation, effects of 600 tides, sudden storms and floods and local water diversions and runoff. A dy-601 namic, time-varying CFD model allows us to model changes in flows that occur as inflows change. In general, a dynamic model will be necessary to correctly 603 decompose drag and locomotion forces when the flow field changes appreciably over time. Not accounting for changes in flow will lead to biased estimates of 605 these components.

After we validated that model against empirical flow measurements, we used 607 flow estimates, along with observed fish migration trajectories, to infer the drag 608 and locomotory forces that produced observed fish accelerations. Rather than 609 prescribing an ad hoc model of locomotion behavior, we used a flexible recur-610 rent neural network model (the LSTM-NN) to describe how flow cues and past 611 behavior influence locomotion behavior in the near future. Importantly, this 612 approach provides accurate near-term forecasts of migrant behavior on out-of-613 sample data. Thus, our model both captures observed patterns of locomotion in 614 complex flows, and is capable of making accurate out-of-sample predictions to evaluate hypothesis about the implications of migratory behavior across space 616 and over ranges of environmental conditions (e.g., Fig. 5).

To predict swimming behavior, we relied on a flexible multivariate time series method. Multivariate time series analysis methods such as the LSTM-NN have become popular in many fields including healthcare (Kang and Choi,

2014), phoneme classification (Kang and Choi, 2005), and activity and action recognition (Pavlovic, Frey, and Huang, 1999, Geurts, 2001, Fu, 2015, Yu 622 and Lee, 2015). In our analysis, the LSTM-NN model of swimming behavior 623 revealed that knowledge of the flow environment the animal experiences as it 624 moves can allow one to make accurate out-of-sample forecasts of a fish's future 625 movements, at least over short timescales (e.g. 2s-30s). This suggests not only 626 that features of the flow influence the movement decisions animals make as they 627 migrate (Liao, 2007, Oteiza et al., 2017), but also that the behavioral rules 628 or "behavioral algorithms" (Hein et al., 2020) that relate flow to locomotion behavior are at least reasonably similar, both across individual animals, and 630 over the range of time periods included in our study. We believe this workflow of building data-driven models of behavior and validating predictions of 632 those models on out-of-sample data is crucial, given that our understanding of how animals perceive and respond to sensory cues during migration is still far 634 from complete. The flexibility of recurrent neural networks frees our approach, 635 at least to some extent, from assumptions about the precise functional form 636 relating flow variables to the swimming behavior of migrants. However, one 637 disadvantage of using a highly flexible framework like LSTM-NN to relate envi-638 ronmental variables to fish behavior is that, due to the complexity of the neural 639 network model structure, there is no compact symbolic representation of the functional relationships between input and output variables (Martin, Munch, 641 and Hein, 2018). We expect future studies will unpack the patterns described phenomenologically by our LSTM-NN model of movement behavior. In partic-643 ular, it will be insightful to determine whether migration behavior, like some other animal behaviors including predator evasion (Hein et al., 2018) and prey interception (Brighton, Thomas, and Taylor, 2017), can be described accurately by a set of relatively simple control algorithms (Hein et al., 2020). Future work 647

could apply other modeling paradigms (e.g., control theory, neuro-ecological modeling, Brighton, Thomas, and Taylor, 2017, Bar et al., 2015) to address this and other fundamental questions, including (i) which variables most influence locomotion, (ii) whether migratory behavior varies appreciably over time, and (iii) the extent to which different individuals respond to environmental variables in different ways. Notably, all of these questions require estimates of both the behavioral actions taken by individual migrants and the environmental variables experienced by those individuals. Our methodology provides a way to acquire such estimates.

While the overall methodology presented here holds much promise, it nev-657 ertheless has important limitations. Firstly, due to computational limitations on the simulation of turbulent flow, the spatial and temporal resolution of our 659 CFD model is limited. This means that we cannot resolve fine-scale flow at the scale of the migrating fish's body, nor can we fully resolve temporal fluctuations 661 in flow due to turbulence. This makes it challenging to directly link our model 662 of locomotion behavior with biomechanical (e.g., Lighthill, 1971, Bandyopad-663 hyay, 2002; Cui et al., 2017) or behavioral models (e.g. Oteiza et al., 2017) 664 that describe movement of the migrant's body. Nevertheless, our model does 665 have the ability to resolve larger features in the flow on the spatial scale of tens 666 of body lengths. Such features include gradients in water velocity near channel banks and zones of strong recirculation (e.g., see Fig. 2). This allowed us 668 to conclude, for example, that effects of these features on migratory behavior can be significant (Fig. 5). A second limitation of our approach is due to the 670 tracking data themselves. Tracking data were acquired through hydrophone detections of animals implanted with acoustic transmitters. These data therefore 672 have limited spatial resolution and the status of tagged animals are unknown (e.g., tags from fish consumed by larger predatory fish can still be detected by 674

the hydrophone array). Such limitations are worth considering when choosing a tag technology to use for studies that will combine tracking and physical mod-676 eling to study migratory movement behavior. Another important consideration 677 is that our framework cannot fully address the question of whether high or low 678 flow conditions are more favorable for migration because it does not consider 679 how energy use trades off with other potentially important quantities related to migration success such as the travel time through regions of high predation risk 681 (Anderson, Gurarie, and Zabel, 2005). The times taken by fish to traverse our 682 entire study region were longer, on average, when overall flow was weak (mean of 63 minutes for trajectories experiencing the weakest 10% of flows) than when 684 overall flow was strong (51 minutes for trajectories experiencing strongest 10% of flows). However, variability in this trend was significant. Nevertheless, travel 686 time and other tradeoffs could be included in our framework by integrating additional data sources (e.g. predation risk data). 688

Despite its limitations, our framework can be used to gain traction on questions that have fascinated migration biologists for many years. Many such 690 questions relate to how migrants use energy as they move through a landscape. 691 As demonstrated in Fig. 5, our methodology has much potential to address 692 these types of questions. For example, when applied to distinct environmental 693 conditions observed in our data set, locomotion force predictions revealed that 694 fish generally spend far more energy moving through the landscape when the 695 overall rate of flow is high than when the rate of flow is low, despite the fact that the net flow direction is aligned with the direction of migration. Our analysis 697 provides additional insights into the cause of this pattern; when fish swim in slow currents their movements are generally oriented uniformly relative to the 699 flow with a slight bias toward alignment in the direction of flow (see Appendix A). On the other hand, when migrants move through high speed currents, their 701

movements are primarily oriented against the flow or laterally relative to the
direction of flow. These lateral and opposing movements require greater power
output. It is also important to note our methodology is in no way limited to
the study of migratory movements. Both swimming and flying animals modulate short-term movement behavior in response to local environmental flows
(Scacco et al., 2019, Shepard, Ross, and Portugal, 2016 and James, 2007). The
same methodology presented here can be applied to study animal movement
behaviors beyond the context of migration.

In this work, we have presented a general methodology for merging data 710 and modeling of environmental currents with tracking data to understand an-711 imal migratory behavior. Our approach extends more traditional methods in migration biology, which have often either ignored interactions with wind and 713 water currents, or modeled these interactions in simple ways that are not fully informed by physical data (e.g., Alexander, 1998, Pennycuick, 2003, Hein, Hou, 715 and Gillooly, 2012, Stier et al., 2014). We believe our framework has the poten-716 tial to shed new light on how migrants interact with wind and water currents 717 and how behavior and biophysics interact to determine the costs and benefits 718 of different migratory strategies and environmental conditions. 719

20 Acknowledgements

We thank the California Department of Water Resources (Jacob McQuirk) for providing flow and tracking data, U.S. Geological Survey California Water Science Center (Jon Burau) for technical information related to ADCP data, and HTI Sonar (Sam Johnston) for technical information related to fish tracking data. We also thank M. Celis and A. Fahimipour for technical support with computing and for helpful suggestions on the manuscript, and participants in "Data-theory seminar" for suggestions that improved this work. This project

was supported, in part, through the California Department of Fish and Wildlife from the Water Quality, Supply and Infrastructure Improvement Act of 2014 (CA Department of Fish and Wildlife grant No. P1896007-01), the National Oceanic and Atmospheric Administration High Performance Computing and Communications Program, and the National Science Foundation (IOS Grant 1855956).

Data Accessibility Statement

735 Intended location for data archive: https://datadryad.org/

Authors' contributions statement

Simone Olivetti, Michael A. Gil, Vamsi K. Sridharan, and Andrew M. Hein conceived the ideas and designed methodology; Vamsi K. Sridharan and Andrew
M. Hein pre-processed movement and hydrologic datasets; Simone Olivetti constructed CFD and LSTM models and carried out all analyses with input from all
authors. Simone Olivetti and Andrew M. Hein led the writing of the manuscript.
All authors contributed critically to the drafts and gave final approval for publication.

References

Abadi, M. et al. (2015). TensorFlow: Large-Scale Machine Learning on Heterogeneous Systems. Software available from tensorflow.org. URL: https: //www.tensorflow.org/.

- AECOM (2015). An evaluation of juvenile salmonid routing and barrier effec-
- tiveness, predation, and predatory fishes at the Head of Old River. ICF In-
- ternational, and Turnpenny Horsefield Associates.
- Alerstam, T., Chapman, J. W., Bäckman, J., Smith, A. D., Karlsson, H., Nils-
- son, C., Reynolds, D. R., Klaassen, R. H. G., and Hill, J. K.. (2011). "Con-
- vergent patterns of long-distance nocturnal migration in noctuid moths and
- passerine birds". In: Proceedings of The Royal Society. DOI: https://doi.
- org/10.1098/rspb.2011.0058.
- Alexander, R. M. (1998). "When is migration worthwhile for animals that walk,
- swim or fly?" In: Avian Biology 29, pp. 387–394. DOI: http://dx.doi.org/
- 758 10.1242/jeb.015024.
- Altché, F. and De La Fortelle, Arnaud (2017). "An LSTM network for highway
- trajectory prediction". In: 2017 IEEE 20th International Conference on In-
- telligent Transportation Systems (ITSC). DOI: http://doi.org/10.1109/
- 762 ITSC.2017.8317913.
- Anderson, J.J., Gurarie, E., and Zabel, R.W. (2005). "Mean free-path length
- theory of predator-prey interactions: Application to juvenile salmon migra-
- tion". In: Ecological Modelling, pp. 196-211. DOI: https://doi.org/10.
- 766 1016/j.ecolmodel.2005.01.014.
- Arenas, A., Politano, M., Weber, L., and Timko, M. (2015). "Analysis of move-
- ments and behavior of smolts swimming in hydropower reservoirs". In: Eco-
- logical Modelling. DOI: https://doi.org/10.1016/j.ecolmodel.2015.
- 770 05.015.
- Arya, S., Mount, D. M., Netanyahu, N. S., Silverman, R., Wu, A., and Wu, A. Y.
- (1998). "An optimal algorithm for approximate nearest neighbor searching
- in fixed dimensions". In: ACM. DOI: https://doi.org/10.1145/293347.
- 774 293348.

- Bandyopadhyay, P. R. (2002). "Maneuvering Hydrodynamics of Fish and Small
- Underwater Vehicles". In: Integrative & Comparative Biology. DOI: https:
- //doi.org/10.1093/icb/42.1.102.
- Bar, N.S., Skogestad, S., Marcal, J.M., Ulanovsky, N., and Yovel, Y. (2015). "A
- sensory-motor control model of animal flight explains why bats fly differently
- in light versus dark". In: $PLoS\ Biol.\ 13.\ DOI:\ 10.1371/journal.pbio.$
- 781 1002046.
- Boning, C.W., Dispert, A., Visbeck M.and Rintoul, S.R., and Schwarzkopf, F.U.
- 783 (2008). "The response of the Antarctic Circumpolar Current to recent cli-
- mate change". In: Nature Geoscience 1, pp. 864-869. DOI: http://dx.doi.
- org/10.1038/ngeo362.
- Brighton, Caroline H., Thomas, Adrian L. R., and Taylor, Graham K. (2017).
- "Terminal attack trajectories of peregrine falcons are described by the pro-
- portional navigation guidance law of missiles". In: Proceedings of the Na-
- tional Academy of Sciences 114.51, pp. 13495-13500. DOI: 10.1073/pnas.
- 790 1714532114.
- Cui, Z., Gu, X., Li, K., and Jiang, H. (2017). "CFD Studies of the Effects
- of Waveform on Swimming Performance of Carangiform Fish". In: Applied
- ⁷⁹³ Science. DOI: https://doi.org/10.3390/app7020149.
- Dabiri, J. O. (1993). "Migration by soaring or flapping flight in birds: the relative
- importance of energy cost and speed." In: *Phil. Trans. R. Soc.* DOI: https:
- 796 //doi.org/10.1098/rstb.1993.0164.
- De Lucas, M., Janss, G.F., and Ferrer, M. (2004). "The effects of a wind farm
- on birds in a migration point: the Strait of Gibraltar." In: $Biodiversity \ \mathcal{E}$
- 799 Conservation 13, pp. 395-407. DOI: https://doi.org/10.1111/1365-
- 2664.13107.

- Deshpande, S. S., Anumolu, L., and Trujillo, M. F. (2012). "Evaluating the per-
- formance of the two-phase flow solver interFoam". In: Computational science
- 803 & discovery. DOI: http://dx.doi.org/10.1088/1749-4699/5/1/014016.
- Dingle, H. (2015). Migration: The Biology of Life on the Move. Oxford Schol-
- arship Online. Oxford. ISBN: 9780199640386.
- Flack, A., Nagy, M., Fiedler, W., Couzin, I.D., and Wikelski, M. (2018). "From
- local collective behavior to global migratory patterns in white storks". In:
- Science 360, pp. 911-914. DOI: http://dx.doi.org/10.1126/science.
- 809 aap7781.
- Friedrich, K., Lundquist, J. K., Aitken, M., Kalina, E. A., and Marshall, R. F.
- 811 (2012). "Stability and turbulence in the atmospheric boundary layer: A com-
- parison of remote sensing and tower observations." In: Geophysical Research
- Letters. DOI: https://doi.org/10.1029/2011GL050413.
- Fu, Y. (2015). Human activity recognition and prediction. Springer.
- 815 Gao, Z., Andersson, H. I., Dai, H., Jiang, F., and Zhao, L. (2015). "A new
- 816 Eulerian-Lagrangian agent method to model fish paths in a vertical slot
- fishway". In: Ecological Engineering. DOI: https://doi.org/10.1016/j.
- ecoleng.2015.12.038.
- Geurts, P. (2001). Pattern extraction for time series classification. Springer,
- pp. 115–127.
- Gisen, D. C., Weichert, R. B., and Nestler, J. M. (2016). "Optimizing attraction
- flow for upstream fish passage at a hydropower dam employing 3D Detached-
- Eddy Simulation". In: *Ecological Engineering*. DOI: https://doi.org/10.
- 1016/j.ecoleng.2016.10.065.
- Goodwin, R. A., Politano, M., Garvin, J. W., Nestler, J. M., Hay, D., Anderson,
- J. J., Weber, L. J., Dimperio, E., Smith, D. L., and Timko, M. (2014).

- "Fish navigation of large dams emerges from their modulation of flow field
- experience". In: *PNAS*. DOI: https://doi.org/10.1073/pnas.1311874111.
- Gualtieri, C., Ianniruberto, M., Filizola, N., Santos, R., and Endreny, T. (2019).
- $^{\rm 830}$ $\,$ "A 3D analysis of spatial habitat metrics about the confluence of Negro and
- Solimões rivers, Brazil". In: *Ecohydology*.
- Hein, A.M., Altshuler, D.L., Cade, D.E., Liao, J. C., Martin, B.T., and Taylo,
- G.K. (2020). "An Algorithmic Approach to Natural Behavior". In: Current
- Biology. DOI: https://doi.org/10.1016/j.cub.2020.04.018.
- 835 Hein, A.M., Gil, M.A., Twomey, C.R., Couzin, I.D., and Levin, S.A. (2018).
- "Conserved behavioral circuits govern high-speed decision-making in wild
- fish shoals". In: Proceedings of the National Academy of Sciences. DOI: https:
- //doi.org/10.1073/pnas.1809140115.
- Hein, A.M., Hou, C., and Gillooly, J.F. (2012). "Energetic and biomechanical
- constraints on animal migration distance". In: *Ecology letters*, pp. 104–110.
- DOI: http://doi.org/10.1111/j.1461-0248.2011.01714.x.
- Hoerner, S.F. (1965). Fluid-dynamic drag: theoretical, experimental and statis-
- tical information. Published by the Author. ISBN: 9780123742995.
- Hughey, L., Hein, A. M., Strandburg-Peshkin, A., and Jensen, F. (2018). "Chal-
- lenges and solutions for studying collective animal behavior in the wild". In:
- Phil. Trans. Roy. Soc. By. DOI: https://doi.org/10.1098/rstb.2017.
- 847 0005.
- James, C. L. (2007). "A review of fish swimming mechanics and behaviour in
- altered flows". In: Phil. Trans. R. Soc. DOI: https://doi.org/10.1098/
- rstb.2007.2082.
- Jimenez, J. and Moser, R.D. (1998). A Selection of Test Cases for the Valida-
- tion of Large-Eddy Simulations of Turbulent Flows. North Atlantic Treaty
- Organization, Advisory Group for Aerospace Research Development.

- 854 Kang, H. and Choi, S. (2005). "Framewise phoneme classification with bidirec-
- tional LSTM and other neural network architectures". In: Neural Networks,
- pp. 602-610. DOI: https://doi.org/10.1016/j.neunet.2005.06.042.
- 857 (2014). "Bayesian common spatial patterns for multi-subject EEG classifi-
- cation". In: Neural Networks, pp. 39-50. DOI: https://doi.org/10.1016/
- j.neunet.2014.05.012.
- Kellnerová, R., Fuka, V., Uruba, V., Jurčáková, K., Nosek, Š., Chaloupecká, H.,
- and Jaňour, Z. (2018). "On street-canyon flow dynamics: Advanced valida-
- tion of LES by time-resolved PIV." In: Atmosphere. DOI: https://doi.org/
- 863 10.3390/atmos9050161.
- Killen, S. S., Glazier, D. S., Rezende, E. L., Clark, T. D., Atkinson, D., Willener,
- A. S. T., and Halsey, L. G. (2016). "Ecological Influences and Morphologi-
- cal Correlates of Resting and Maximal Metabolic Rates across Teleost Fish
- Species". In: The American Naturalist.
- Kimmerer, W., R., Avent S., M., Bollens S., F., Feyrer, F., Grimaldo L., B.,
- Moyle P., M., Nobriga, and T., Visintainer (2005). "Variability in Length-
- Weight Relationships Used to Estimate Biomass of Estuarine Fish from Sur-
- vey Data". In: Transactions of the American Fisheries Society. DOI: https:
- //doi.org/10.1577/T04-042.1.
- 873 Kling, M.M. and Ackerly, D.D. (2020). "Global wind patterns and the vul-
- nerability of wind-dispersed species to climate change". In: Nature Climate
- change 10, pp. 868-875. DOI: http://dx.doi.org/10.1038/s41558-020-
- 876 0848-3.
- Lacey, R. W. J., Neary, V. S., Liao, J. C., Enders, E. C., and Tritico, H. M.
- 878 (2012). "The IPOS framework: Linking fish swimming performance in al-
- tered flows from laboratory experiments to rivers". In: River Research and
- Applications, pp. 429-443. DOI: https://doi.org/10.1002/rra.1584.

- Liao, J. C. (2007). "A review of fish swimming mechanics and behaviour in al-
- tered flows". In: Philosophical Transactions of the Royal Society B: Biological
- Sciences.
- Lighthill, M. J. (1971). "Large-amplitude elongated-body theory of fish locomo-
- tion". In: Proceedings of The Royal Society. DOI: https://doi.org/10.
- 886 1098/rspb.1971.0085.
- Ling, H., E., McIvor G., Nagy, G., MohaimenianPour, S., Vaughan, R. T., Thorn-
- ton, A., and Ouellette, N. T. (2018). "Simultaneous measurements of three-
- dimensional trajectories and wingbeat frequencies of birds in the field". In:
- Journal of The Royal Society Interface. DOI: https://doi.org/10.1098/
- rsif.2018.0653.
- Madala, S., Satyanarayana, A. N. V., Srinivas, C. V., Kumar, M. E. A., and Mar-
- shall, R. F. (2015). "Stability and turbulence in the atmospheric boundary
- layer: A comparison of remote sensing and tower observations." In: Geophys-
- ical Research Letters. DOI: https://doi.org/10.1016/j.atmosenv.2015.
- 896 02.059.
- Martin, B.T., Munch, S.B., and Hein, A.M. (2018). "Reverse-engineering eco-
- logical theory from data." In: Proc. R. Soc. B. DOI: http://dx.doi.org/
- 899 10.1098/rspb.2018.0422.
- Martin, B.T., Nisbet, R.M., Pike, A., Michel, C.J., and Danner, E.M (2015).
- "Sport science for salmon and other species: ecological consequences of metabolic
- power constraints." In: Ecology Letters 18, pp. 535–544.
- Martin, J.E., Politano, M.S., Prakash, S., Carrica, P.M., and Markfort, C.D.
- 904 (2017). "Optimizing Bat Carcass Search Areas Using a CFD-Lagrangian
- 905 Modeling Approach." In: Technical report to Mid American Energy Company
- 906 414.

- Menter, F. R. (1994). "Two-equation Eddy-viscosity turbulence models for engi-
- neering applications". In: AIAA Journal. DOI: https://doi.org/10.2514/
- 909 3.12149.
- North, E. W., Schlag, Z., Hood, R. R., Li, M., Zhong, L., Gross, T., and Kennedy,
- V. S. (2008). "Vertical swimming behavior influences the dispersal of simu-
- lated oyster larvae in a coupled particle-tracking and hydrodynamic model of
- Chesapeake Bay". In: Marine Ecology Progress 359, pp. 99–115. DOI: https:
- 914 //doi.org/10.3354/meps07317.
- Oteiza, P., Odstrcil, I., Lauder, G., Portugues, R., and Engert, F. (2017). "A
- novel mechanism for mechanosensory-based rheotaxis in larval zebrafish".
- In: *Nature*. DOI: https://doi.org/10.1038/nature23014.
- Pavlovic, V., Frey, B. J., and Huang, T. S. (1999). "Time-series classification
- using mixed-state dynamic Bayesian networks". In: $IEEE\ computer\ society$
- conference, pp. 609-615. DOI: https://doi.org/10.1016/j.neunet.2005.
- 921 06.042.
- Pennycuick, C.J. (2003). "The concept of energy height in animal locomotion:
- separating mechanics from physiology". In: Theoretical Biology 224, pp. 189–
- 203. DOI: http://dx.doi.org/10.1016/S0022-5193(03)00157-7.
- 925 (2008). Modelling the flying bird. Theoretical Ecology. Academic Press. ISBN:
- 9780123742995.
- Ramón, C. L., Acosta, M., and Rueda, F. J. (2018). "Hydrodynamic Drivers
- of Juvenile-Salmon Out-Migration in the Sacramento River: Secondary Cir-
- culation". In: J. Hydraul. Eng. DOI: https://ascelibrary.org/doi/10.
- 930 1061/%28ASCE%29HY.1943-7900.0001484.
- Reddy, G., Celani, A., Sejnowski, T. J., and Vergassola, M. (2016). "Learning
- to soar in turbulent environments". In: Proceedings of the National Academy
- of Sciences. DOI: https://doi.org/10.1073/pnas.1606075113.

- 934 Scacco, M., Flack, A., Duriez, O., Wikelski, M., and Safi, K. (2019). "Static
- landscape features predict uplift locations for soaring birds across Europe".
- In: Royal Society open science. DOI: https://doi.org/10.1098/rsos.
- 937 181440.
- Shepard, E. L. C., Ross, A. N., and Portugal, S. J. (2016). "Moving in a moving
- medium: new perspectives on flight". In: Phil. Trans. R. Soc. DOI: https:
- 940 //doi.org/10.1098/rsos.181440.
- Silva, A.T., Lucas, M.C., Castro-Santos, T., Katopodis, C., Baumgartner, L.J.,
- Thiem, J.D., Aarestrup, K., Pompeu, P.S., O'Brien, G.C., Braun, D.C., and
- Burnett, N.J. (2018). "The future of fish passage science, engineering, and
- practice." In: Fish and Fisheries 19, pp. 340-362. DOI: http://dx.doi.
- org/10.1111/faf.12258.
- Smith, R.J.F (2012). The control of fish migration. Zoophysiology. Springer.
- 947 ISBN: 9783642823480.
- 948 Sridharan, V.K., Monismith, S.G., O.B., Fringer, and Fong, D.A. (2006). "Eval-
- uation of the Delta Simulation Model-2 in Computing Tidally Driven Flows
- 950 in the Sacramento-San Joaquin Delta". In:
- 951 Stier, A.C., Hein, A.M., Parravicini, V., and Kulbicki, M. (2014). "Larval dis-
- persal drives trophic structure across Pacific coral reefs". In: Nature Com-
- munications. DOI: https://doi.org/10.1038/ncomms6575.
- 954 Stumpner, P. (2013a). "Memo on HORB 2009 and 2011 Hydrodynamic Data
- Processing and Interpolation". In: Task No. TEMBAR-07. AECOM Tech-
- nical Services Inc. Sacramento, CA.
- 957 (2013b). "Memo on Head of Old River Deployment 2012". In: AECOM Tech-
- nical Services Inc. Sacramento, CA.
- Thorstad, E.B., Økland, F., Aarestrup, K., and Heggberget, T.G. (2008). "Fac-
- tors affecting the within-river spawning migration of Atlantic salmon, with

- emphasis on human impacts." In: Reviews in Fish Biology and Fisheries 18,
- pp. 345-371. DOI: http://dx.doi.org/10.1007/s11160-007-9076-4.
- Wagenbrenner, N. S., Forthofer, J. M., Lamb, B. K., Shannon, K. S., and But-
- ler, B. W. (2016). "Downscaling surface wind predictions from numerical
- weather prediction models in complex terrain with WindNinja." In: Atmo-
- spheric Chemistry and Physics. DOI: https://doi.org/10.5194/acp-16-
- 967 5229-2016.
- 968 Wang, R.F., Ateljevich, E., Fregoso, T.A., and Jaffe, B.E. (2018). "A revised
- continuous surface elevation model for modeling." In: Methodology for Flow
- and Salinity Estimates in the Sacramento-San Joaquin Delta and Suisun
- 971 Marsh: 39th Annual Progress Report. Bay-Delta Office, California Depart-
- ment of Water Resources and Pacific Coastal and Marine Science Center,
- United States Geological Survey, pp. 125–170.
- 974 Weber, L. J., Goodwin, R. A., Li, S., Nestler, J. M., and Anderson, J. J. (2006).
- "Application of an Eulerian-Lagrangian-Agent method (ELAM) to rank al-
- ternative designs of a juvenile fish passage facility." In: Hydroinformatics 8.
- poi: https://doi.org/10.2166/hydro.2006.006.
- 978 Weller, H. G. and Tabor, G. (1998). "A tensorial approach to computational
- continuum mechanics using object-oriented techniques." In: Computers in
- Physics. DOI: https://doi.org/10.1063/1.168744.
- 981 Williams, J. G (2006). "Central Valley salmon: a perspective on Chinook and
- steelhead in the Central Valley of California". In: San Francisco Estuary and
- Watershed Science 4.3.
- Winstral, A., Jonas, T., and Helbig, N. (2017). "Statistical downscaling of grid-
- ded wind speed data using local topography." In: Journal of Hydrometeorol-
- ogy. DOI: https://doi.org/10.1175/JHM-D-16-0054.1.

```
Xue, H., Huynh, D. Q., and Reynolds, M. (2018). "An LSTM network for highway trajectory prediction". In: SS-LSTM: A Hierarchical LSTM Model for Pedestrian Trajectory Prediction. DOI: http://doi.org/10.1109/WACV.
2018.00135.
Yu, Z. and Lee, M. (2015). "Real-time human action classification using a dynamic neural model". In: Neural Networks, pp. 29-43. DOI: https://doi.org/10.1016/j.neunet.2015.04.013.
```

Appendix A: Drag coefficient, resting metabolic

² rate, and swimming orientation relative to flow

- To estimate the dragging force on each fish, we required an estimate of the drag
- 4 coefficient for these animals. The average fish length was L=0.112m (AE-
- 5 COM, 2015). The drag coefficient was estimated using a formula for Reynolds
- $_{6}$ numbers $R_{e} > 2000$ based on fish length and fish relative velocity, $C_{d} =$
- $_{7}$ $\,$ 493.9/Re $^{0.922}$ (Arenas et al., 2015). Given the average fish relative velocity, $v_{r}=$
- $_{8}$ 0.34m/s, average fish length L=0.112m and water density $\rho_{w}=999.06kg/m^{3}$
- $_{9}$ we have $C_{d}=0.033.$ The fish wetted area A_{f} is estimated using the formula
- $A_f = 0.28L^{2.11} = 0.0026m^2$ (Webb, 1976).
- Mean fish length was also used to estimate resting metabolic rate for the
- locomotory scope calculation. We first used length to estimate average mass
- using scaling a scaling relationship for juvenile Chinook Salmon (Kimmerer et
- al., 2005): $m_{fish}=(10^{-3})(1.8\times 10^{-3})L^{3.44}$, which gave an estimate of $m_{fish}\approx 1.000$
- $_{15}$ 0.02kg. The resting metabolic rate was calculated using the formula: RMR =
- $m_{fish}^{0.95} 10^{-1.385+0.021T}$, where T is the water temperature (degrees Celsius, Killen
- 17 et al., 2016).
- Fig. 5c (main text) illustrates that fish swim in ways that can cause them
- to expend far more energy on locomotion when swimming in strong flows than
- when the overall rate of flow through the system is weak. To better understand
- the source of this pattern, we can use the observed tracks along with CFD-
- derived estimates of flow direction to determine how fish orient to local flow in
- 23 low versus high flow conditions. Fig. 1 shows that when the overall rate of flow
- through the system is relatively low, fish movements tend to be oriented more
- $_{25}$ or less uniformly with respect to the direction of flow, with a slight bias in the
- direction of the flow (Fig. 1, left circular histogram). When water currents are

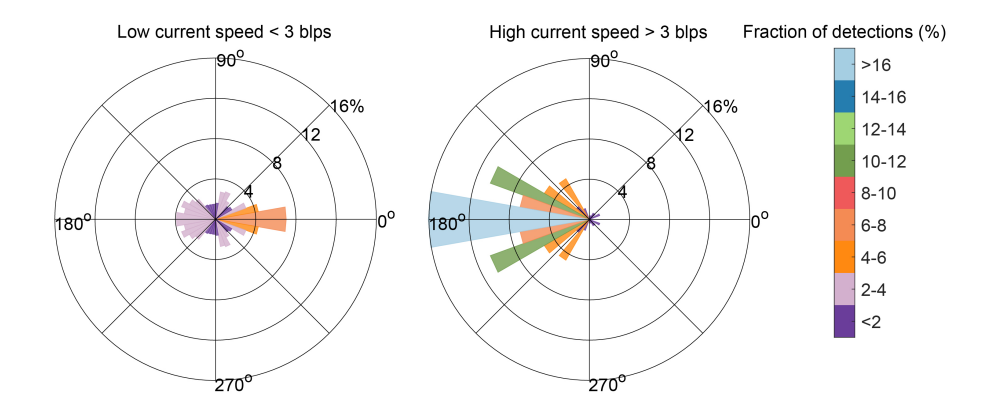


Figure 1: Orientation of fish relative velocity with respect to direction of water flow; low flow regime (left) high flow regime (right). An angle of 0 corresponds to alignment with local water velocity, whereas 180 corresponds to alignment directly against local water velocity. Color scale shows fraction of observations falling into each orientation bin.

- 27 fast, fish movements tend to be oriented opposite the flow or at at angles that
- would move them laterally relative to the flow direction (Fig. 1, right circular
- 29 histogram). Thus, rather than moving in the same way under different flow
- 30 conditions, fish tend to move in ways that oppose powerful local flows when the
- overall rate of flow through the system is high, leading to the high predicted
- costs of locomotion under such conditions (Fig. 5 in main text).

33 Appendix B: CFD mesh generation and modeling

34 details

- In this Appendix we give more details regarding the mesh generation and bound-
- ary conditions used for the CFD simulations. We used SnappyHexMesh (Weller
- and Tabor, 1998), the openFOAM meshing tool to generate a preliminary mesh
- which we subsequently trimmed to conform to the bathymetry. The prelimi-
- nary mesh consisted of four blocks (Fig. 2a). Each block comprises of a specific

number of cells (Table 1). Block one is characterized by hexahedral cells with dimensions $0.8m \times 0.64m \times 0.3m$ respectively in the along-stream, lateral and vertical direction. Blocks two and three are characterized by hexahedral cells with dimensions $0.64m \times 0.45m \times 0.3m$ (Fig. 2b). Blocks two and three have a slightly finer mash in comparison with block one because most of the large coherent structures in the flow occur in the regions spanned by these blocks. Block four is at the outlet of the flow domain, and we therefore applied a gentle

	$nx \times ny \times nz$	Total
Block 1	$150\times210\times38$	1145700
Block 2	$150 \times 210 \times 38$	1145700
Block 3	$150 \times 210 \times 38$	1145700
Block 4	$15 \times 210 \times 38$	114570

Table 1: Number of cells for preliminary mesh. $nx \times ny \times nz$: number of cells in x, y and z direction respectively.

stretch to the cells towards the outlet, Fig. 2c. The resulting cells dimensions at 47 the outlet are $2.3m \times 0.45m \times 0.3m$. All the blocks together form a preliminary mesh of 3,551,670 cells. We then adapted the preliminary mesh to the topography of the river using the openFOAM tool snappyHexMesh (Fig. 2d and Fig. 2e). Snapped cells are subject to three consecutive mesh refinements. Hence, 51 the refined snapped cells are three time smaller than the cells from the prelim-52 inary mesh. The refined snapped cells are arbitrary polyhedral cells bounded by arbitrary polygonal faces. Eventually, after the snapping process, the final mesh consists of 17,474,654 cells. Fig. 2f and 2g show the air-water phases initialized; the red and blue colors are the water and the air media respectively; 56 the white color represents the water-air interface. We applied a zero-gradient for the velocity field on the outlet and the atmosphere boundaries, see Fig.2f. In the CFD simulations, we apply no-slip conditions to the velocity field on the riverbed and on the barrier, see Fig. 2g. We initialize the turbulent kinetic energy k at $5.4 \times 10^{-5} m^2/s^2$ and the turbulent kinetic energy dissipation rate ω

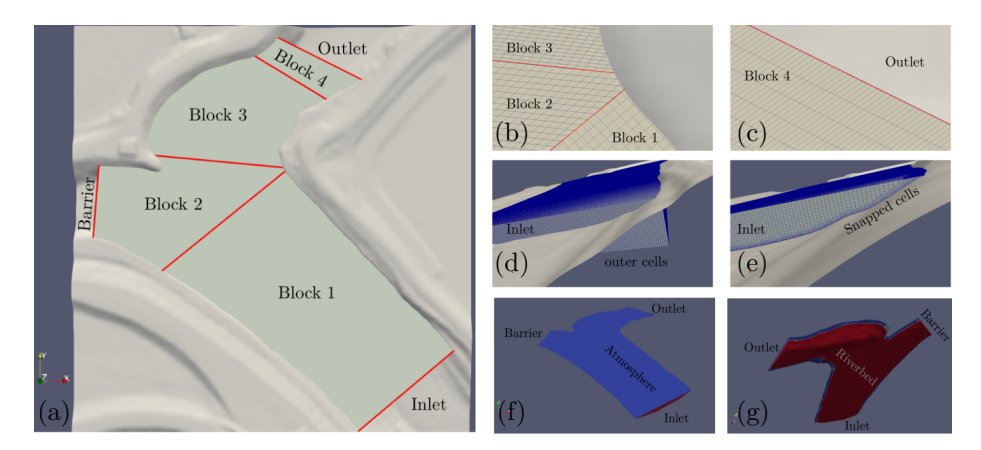


Figure 2: a) Flow domain subdivided in four blocks. b) First 3 contiguous blocks with different mesh resolution. c) Block 4 with a stretch mesh towards the outlet. d) Preliminary mesh with outer cells. d) Final mesh with snapped cells. Boundary and initial conditions: f) Top-down view. g) Down-top view.

- at $2s^{-2}$ over the flow domain. We set the physical properties of the air and water
- 63 media, such as kinematic viscosity and density for a constant temperature of
- 64 15°C (the system is considered isothermal). The density and kinematic viscosity
- for the air layer are $\rho_a = 1.225 kg/m^3$ and $\mu_a = 1.48 \times 10^{-5} m^2/s$, respectively.
- The density and kinematic viscosity for the water layer are $\rho_w = 999.06 kg/m^3$
- and $\mu_w = 1.138 \times 10^{-6} m^2/s$, respectively. We set the time step for the simulation
- to 1s to ensure numerical stability.

⁶⁹ Appendix C. LSTM-NN parameterization and struc-

70 ture selection

- To select the structure of the LSTM architecture, one must select the number
- 72 of cells to include. We did this by evaluating a range of cell counts and mea-
- suring the prediction bias of models with these different structures. In Fig. 3
- each dot represents a LSTM-NN architecture with an assigned number of cells
- while the corresponding mean values of ΔF_{Lx} and ΔF_{Ly} are displayed on the

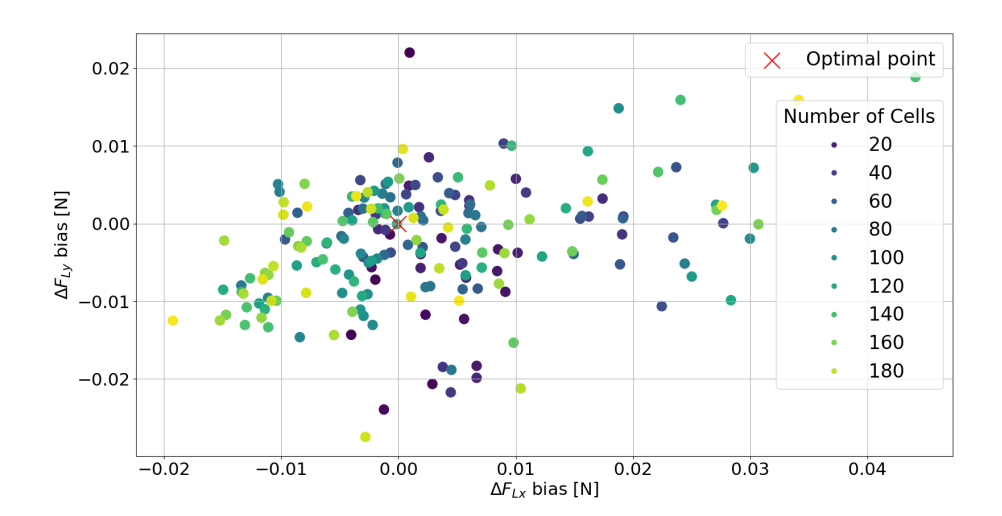


Figure 3: Optimal architecture based on kNN test. Average error for the x locomotion component on the horizontal axes; average error for the y locomotion component on the vertical axes. Every dot corresponds to a specific number of cell in the LSTM architecture. Red cross is the optimal configuration with zero error for both error locomotion components.

 $_{76}$ horizontal and vertical axis respectively. The optimal architecture correspond

77 to the number of cells that produce the minimum error for ΔF_{Lx} and ΔF_{Ly} .

In this case an LSTM with 122 cells is the optimal configuration, red cross in

⁷⁹ Fig. 3.

An LSTM-NN consists of a cascade of interconnected LSTM cells (Fig. 1e main text). A key feature of LSTM cells is the presence of an internal state which serves as a "memory", C(t), associated with each cell in the network. A

generic cell receives three variables: the previous cell's memory state C(t-1),

the previous cell's output h(t-1) and the current sensory input variables, x(t).

The cell then performs different internal operations using so-called "gates" to

produce two outcomes: the current memory state C(t) and the current output

h(t). The gates performing the internal operation are the following:

• Selection gate: select the information to forget. This gate uses x(t) and the previous cell's output h(t-1) employing a sigmoid function, hence,

- $f_t = \sigma(W_f[h(t-1), x_t] + b_f)$, where W_f and b_f are weight and bias coefficients;
- Input gate: select the information to remember. This step consists of two parts: first, a sigmoid function decides which values to update, $i_t = \sigma(W_i[h_{t-1}, x_t] + b_i)$. Next, a tanh function creates a vector of new candidate values, $\widetilde{C}(t)$, that will be added to the state; $\widetilde{C}(t) = \tanh(W_c[h_{t-1}, x_t] + b_c)$.
- Memory gate: update the previous memory state C(t-1) into a new memory state C(t) with the operation $C(t) = f_t C_{t-1} + i_t \widetilde{C}(t)$. The product $f_t C_{t-1}$ "forgets" information from the previous memory state C(t-1). The product $i_t \widetilde{C}(t)$ selects new information to "remember."
- Update gate: finally the output cell is computed as $h(t) = o_t \tanh(C_t)$ where $o_t = \sigma(W_o[h_{t-1}, x_t] + b_o)$.

$_{103}$ Appendix D. Bathymetry of the investigated site.

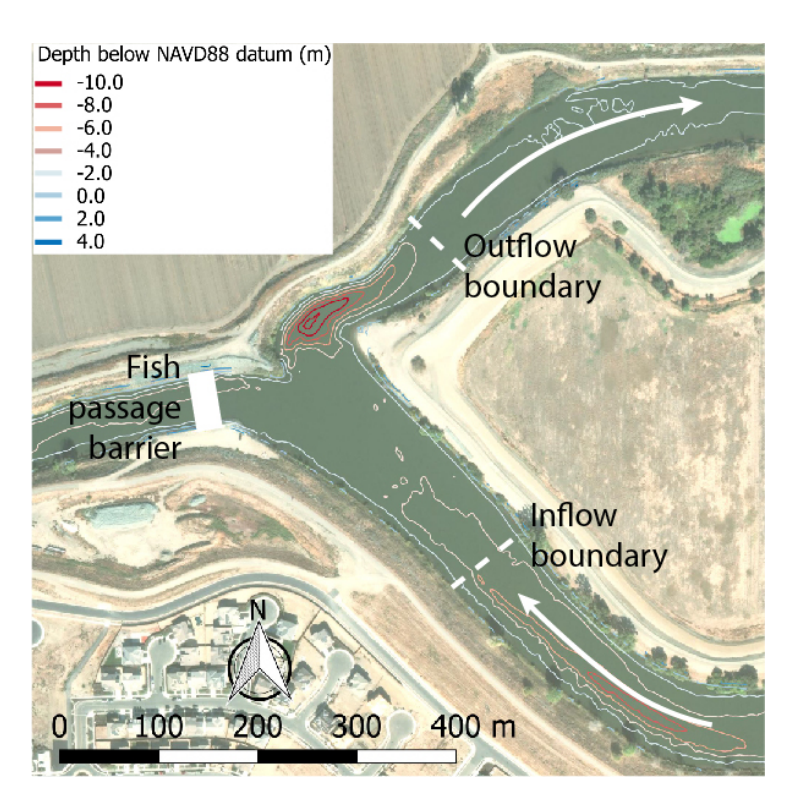


Figure 4: Bathymetry of the investigated site.

104